Journal of Electrical Engineering & Technology Vol. 6, No. 5, pp. 647~657, 2011 **647**
http://dx.doi.org/10.5370/JEET.2011.6.5.647

Sliding Mode Control with Fixed Switching Frequency for Four-wire Shunt Active Filter

Farid Hamoudi†, A. Aziz Chaghi*, Hocine Amimeur and El Kheir Merabet****

Abstract – The present paper proposes a sliding mode control with fixed switching frequency for three-phase three-leg voltage source inverter based four-wire shunt active power filter. The aim is to improve phase current waveform, neutral current mitigation, and reactive power compensation in electric power distribution system. The performed sliding mode for active filter current control is formulated using elementary differential geometry. The discrete control vector is deduced from the sliding surface accessibility using the Lyapunov stability. The problem of the switching frequency is addressed by considering hysteresis comparators for the switched signals generation. Through this method, a variable hysteresis band has been established as a function of the sliding mode equivalent control and a predefined switching frequency in order to keep this band constant. The proposed control has been verified with computer simulation which showed satisfactory results.

Keywords: Sliding mode control, Switching frequency, Four-wire active filter, Current harmonics compensation

1. Introduction

At present, the three-phase four-wire active power filters are attracting considerable interest of researchers in the field of power quality conditioning [1]-[9]. Two configurations of voltage source inverter (VSI) can be used to implement three-phase four-wire active filters. The first uses a fourth leg to provide the neutral current. The second configuration uses a conventional three-leg converter with two cascade-connected capacitors in the DC-bus. The neutral wire is connected directly to the midpoint of this bus. Although the four-leg configuration is preferable because of its simple controllability [5], [10], the three-leg configuration which is used in this paper has the advantage of reduced number of semi-conductors.

The computation of compensated components is the first step required in active filter control. It is used to identify the undesirable component to be suppressed and consequently, the additional components needed to compensate the active filter losses. Several control algorithms, such as instantaneous reactive power theory [11], synchronous reference frame [7], and fast Fourier transform method [12] are used in this manner. Subsequently, the VSI is forced to inject these components in the point of common coupling with minimum error and fast response. This requires an appropriate current control method. In this way, the sliding mode control (SMC), which is derived from the theory of variable structure control and known as a discontinuous control technique that takes into account the time varying topology of the controlled system, is naturally suitable to the control systems. Suitability is based on power electronics devices in general [13]-[18] as well as active filter as a particular case of these systems [19]-[21]. Sliding mode control is characterized by simple implementation, fast response, and high robustness. However, the ideal sliding motions imply infinite frequency in the switched signals which is naturally impossible to achieve in practice, where the switching frequency must be finite and stable. The idea of fixed frequency control in power converters has been addressed in several works [22]-[28]. Most of these contributions are based on the relation between the switching frequency and the average control which is also called equivalent control. It has been shown that it is possible to modulate this continuous control to generate the switched signals with fixed frequency by using PWM modulation [23], [29] or Σ-Δ-modulation [18]. In the present paper, the switching signals are generated through hysteresis comparators, which are very popular in current control application and often used in sliding mode implementation, in order to limit the switching frequency. Although simple and extremely robust [30], the switching frequency remains free and varies considerably with respect to the state variables when the hysteresis bandwidth is preliminary fixed.

However, it has been shown in several studies [22], [24]-[27], [30] that it is possible to keep this frequency constant by adopting a variable hysteresis bandwidth. The idea developed in this work consists of implementation of the sliding mode control with varied hysteresis bandwidths

† Corresponding Author: Institute of Electrical and Electronic Engineering, Boumerdès University, Algeria. (f_hamoudi@yahoo.fr)
* LSPIE Laboratory, Batna University, Algeria. (az_chaghi@yahoo.fr)
** Department of Electrical Engineering, Batna University, Algeria.
Received: September 23, 2010; Accepted: March 25, 2011

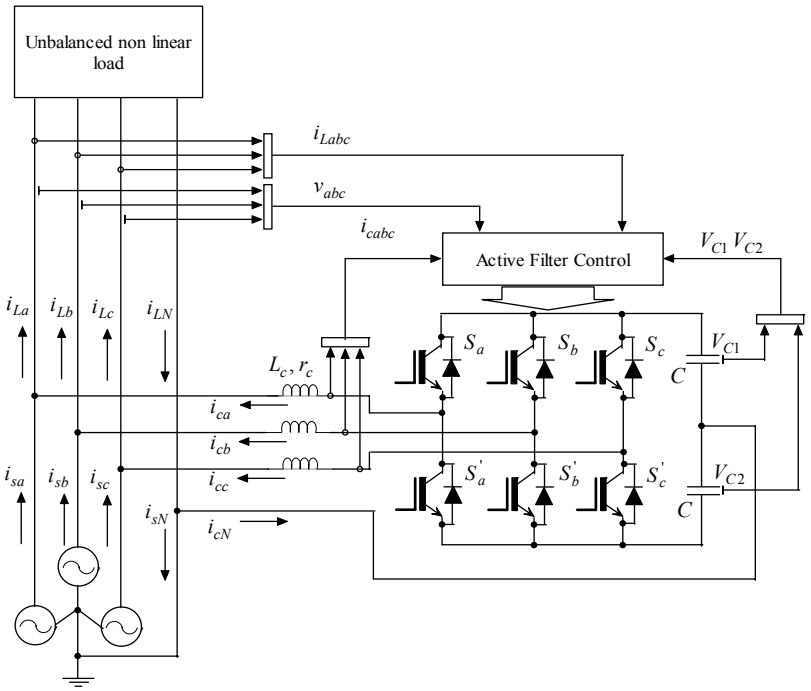

Fig. 1. Three-phase three-leg VSI based four-wire shunt active filter

instead of the switching frequency which is required to be constant.

This paper is divided as follows. A brief description and modeling of the active filter are presented in section 2 while the principle of the compensated components computation is analyzed in section 3. The aim of the paper is discussed in detail in section 4 and the computer simulations are given in section 5. The last section provides the conclusion.

2. System Description and Modeling

Fig. 1 illustrates the basic compensation principle of the four-wire shunt active power filter (SAPF). The power circuit is based on three-phase three-leg controlled current voltage source PWM inverter connected to the grid at the AC side through a passive filter (L_C, r_C). The circuit uses two cascade connected capacitors $C_1 = C_2 = C$ as voltage source at the DC side, with the midpoint connected to the neutral wire of the grid to compensate neutral load current. An unbalanced nonlinear load is considered as a polluting source that draws unbalanced and distorted current i_{Labc} from the main source. The SAPF is controlled to inject compensated current vector i_{cabc} in the grid in order to achieve source current i_{sabc} which is balanced, sinusoidal, and in phase with the fundamental main voltages, while keeping the DC-link voltages V_{C1} and V_{C2} balanced and within an admissible range. To establish the dynamic equations of the system, let us suppose that the power switch S_j can be assumed as ideal. Consequently, the output voltage for each phase j to neutral can be expressed as follows [31]:

$$v_{cj} = d_j V_{C1} - \bar{d}_j V_{C2} \tag{1}$$

$d_j (j = a, b, c)$ are the PWM switching functions given by:

$$d_j = \frac{u_j + 1}{2} \tag{2}$$

where u_j is associated to the power switch states as follows:

$$u_j = 1 \text{ If } S_j \text{on and } S'_j \text{ off}$$
$$u_j = -1 \text{ If } S_j \text{off and } S'_j \text{ on.}$$

Substituting Eq. (2) for Eq. (1), the active filter voltage is subsequently rewritten as follows:

$$v_{cj} = \frac{1}{2} u_j (V_{C1} + V_{C2}) + \frac{1}{2} (V_{C1} - V_{C2}). \tag{3}$$

The DC-bus voltages across the two capacitors are related to u_j and the active filter currents i_{cj} is written as follows:

$$\frac{dV_{C1}}{dt} = \frac{1}{2C} \left(\sum_{j=a,b,c} u_j i_{cj} + \sum_{j=a,b,c} i_{cj} \right) \tag{4}$$

$$\frac{dV_{C2}}{dt} = \frac{1}{2C}\left(\sum_{j=a,b,c} u_j i_{cj} - \sum_{j=a,b,c} i_{cj}\right). \quad (5)$$

From Kirchhoff's voltage law, the interaction between the voltage source inverter and the grid is described by the following differential equation:

$$L_c \frac{di_{cj}}{dt} = -r_c i_{cj} + \frac{1}{2} u_j V_{dc} + \frac{1}{2}(V_{C1} - V_{C2}) - v_j \quad (6)$$

where v_j represents the main voltages at the point of common coupling. Finally, these equations are rearranged under matrix form:

$$\dot{\boldsymbol{x}} = \boldsymbol{A}\boldsymbol{x} + \boldsymbol{B}(\boldsymbol{x})\boldsymbol{u} + \boldsymbol{v} \quad (7)$$

where

$$\boldsymbol{x} = \begin{bmatrix} i_{ca} \\ i_{cb} \\ i_{cc} \\ V_{C1} \\ V_{C2} \end{bmatrix}, \quad \boldsymbol{A} = \begin{bmatrix} -\frac{r_c}{L_c} & 0 & 0 & \frac{1}{2L_c} & -\frac{1}{2L_c} \\ 0 & -\frac{r_c}{L_c} & 0 & \frac{1}{2L_c} & -\frac{1}{2L_c} \\ 0 & 0 & -\frac{r_c}{L_c} & \frac{1}{2L_c} & -\frac{1}{2L_c} \\ \frac{1}{2C} & \frac{1}{2C} & \frac{1}{2C} & 0 & 0 \\ -\frac{1}{2C} & -\frac{1}{2C} & -\frac{1}{2C} & 0 & 0 \end{bmatrix}$$

$$\boldsymbol{B}(\boldsymbol{x}) = \begin{bmatrix} \frac{V_{dc}}{2L_c} & 0 & 0 \\ 0 & \frac{V_{dc}}{2L_c} & 0 \\ 0 & 0 & \frac{V_{dc}}{2L_c} \\ \frac{i_{ca}}{2C} & \frac{i_{cb}}{2C} & \frac{i_{cc}}{2C} \\ \frac{i_{ca}}{2C} & \frac{i_{cb}}{2C} & \frac{i_{cc}}{2C} \end{bmatrix}, \quad \boldsymbol{u} = \begin{bmatrix} u_a \\ u_b \\ u_c \end{bmatrix}, \quad \boldsymbol{v} = \begin{bmatrix} -\frac{v_a}{L_c} \\ -\frac{v_b}{L_c} \\ -\frac{v_c}{L_c} \\ 0 \\ 0 \end{bmatrix}$$

3. Principe of Operation

In four-wire systems, the current drawn by an unbalanced nonlinear load contains positive-sequence, negative-sequence, and zero-sequence harmonic components that can be expressed in $\alpha\beta\gamma$ −frames and arranged in matrix form as follows [32]:

$$\boldsymbol{i_{L\alpha}} = [i^+_{L\alpha 1} \quad i^+_{L\alpha 2} \quad \dots \quad i^+_{L\alpha n} \quad i^-_{L\alpha 1} \quad i^-_{L\alpha 2} \quad \dots \quad i^-_{L\alpha n}]$$
$$\boldsymbol{i_{L\beta}} = [i^+_{L\beta 1} \quad i^+_{L\beta 2} \quad \dots \quad i^+_{L\beta n} \quad i^-_{L\beta 1} \quad i^-_{L\beta 2} \quad \dots \quad i^-_{L\beta n}]$$
$$\boldsymbol{i_{L\gamma}} = [i_{L\gamma 1} \quad i_{L\gamma 2} \quad \dots \quad i_{L\gamma n}].$$

In addition, if the main voltages are supposed to be unbalanced and contain harmonics, then they can be expressed in the same way as:

$$\boldsymbol{v_\alpha} = [v^+_{\alpha 1} \quad v^+_{\alpha 2} \quad \dots \quad v^+_{\alpha n} \quad v^-_{\alpha 1} \quad v^-_{\alpha 2} \quad \dots \quad v^-_{\alpha n}]^T$$
$$\boldsymbol{v_\beta} = [v^+_{\beta 1} \quad v^+_{\beta 2} \quad \dots \quad v^+_{\beta n} \quad v^-_{\beta 1} \quad v^-_{\beta 2} \quad \dots \quad v^-_{\beta n}]^T$$
$$\boldsymbol{v_\gamma} = [v_{\gamma 1} \quad v_{\gamma 2} \quad \dots \quad v_{\gamma n}]^T.$$

Hence, the instantaneous real, imaginary, and zero-sequence powers absorbed by the non linear load are the results from the different interactions between the different harmonics sequences of the load currents and main voltages. Thus, the instantaneous real power components can be expressed in matrix form as follows:

$$\boldsymbol{P_L} = \begin{bmatrix} \boldsymbol{v_\alpha} \\ \boldsymbol{v_\beta} \end{bmatrix} [\boldsymbol{i_\alpha} \quad \boldsymbol{i_\beta}]. \quad (8)$$

This matrix contains all possible combinations between positive and negative-sequences of the main voltages and load currents. It is not difficult to observe that the diagonal elements are in DC form and all the other elements are in AC form. Hence, the DC part of the real power can be expressed as the trace of $\boldsymbol{P_L}$:

$$\bar{p}_L = \sum_{i=1}^{n} \left(v^+_{\alpha i} i^+_{L\alpha i} + v^-_{\alpha i} i^-_{L\alpha i} + v^+_{\beta i} i^+_{L\beta i} + v^-_{\beta i} i^-_{L\beta i}\right). \quad (9)$$

After simplification, Eq. (9) can be written in *abc*− frames as follows:

$$\bar{p}_L = \bar{p}_{Lf} + \bar{p}_{Lh} \quad (10)$$

where

$$\bar{p}_{Lf} = 3V_1^+ I_{L1}^+ \cos(\phi_{V_1^+} - \phi_{I_{L1}^+})$$
$$\bar{p}_{Lh} = \sum_{i=2}^{n} 3\, V_i^+ I_{Li}^+ \cos\left(\phi_{V_i^+} - \phi_{I_{Li}^+}\right) + \sum_{i=1}^{n} 3\, V_i^- I_{Li}^- \cos\left(\phi_{V_i^-} - \phi_{I_{Li}^-}\right).$$

V_i^+, V_i^- and I_{Li}^+, I_{Li}^- are the *rms* values of the positive and negative-sequences of the voltage and current components for the i^{th} harmonic, whereas $\phi_{V_i^+}, \phi_{V_i^-}$ and $\phi_{I_{Li}^+}, \phi_{I_{Li}^-}$ are their respective phase shifts.

Eq. (10) shows that if the SAPF is controlled to provide constant real power $\bar{p}_L$ drawn from the source, then the source currents remain non-sinusoidal because positive and negative sequences of the current that interact with the same sequences at the same frequencies will contribute to a constant real power exchange $\bar{p}_{Lh}$. Consequently, they are not perceived as undesirable components, thus non-

compensated. In conclusion, to guarantee sinusoidal source current, only $\overline{p}_{Lf}$ must be delivered by the source; in other words, the three-phase source currents must contain only fundamental positive-sequence I_{L1}^{+} of the load currents. However, in the active filter operation, active losses in the power switches and passive filter occur that cause variations in the DC-bus voltage. To avoid this situation, these losses must be compensated by drawing an additional active current I_{loss} from the AC source. This is achieved traditionally by the DC-bus voltage controller that generates the reference signal for I_{loss} from the error between the reference value V_{dc}^{*} dc and the measured value V_{dc}. Thus, the peak source current including the DC-bus voltage regulation is:

$$\hat{I}_s = \hat{I}_{L1}^{+} \cos\left(\phi_{V_1^+} - \phi_{I_{L1}^+}\right) + I_{loss.} \tag{11}$$

If I_{loss} is generated by a proportional-integral (PI) controller with k_p and k_p as proportional and integral gains, then:

$$I_{loss} = k_p(V_{dc}^{*} - V_{dc}) + k_i \int (V_{dc}^{*} - V_{dc})\, dt. \tag{12}$$

Subsequently, the resulting instantaneous three-phase source currents are:

$$\begin{aligned} i'_{sa} &= \hat{I}_s \sin(\omega_f t + \delta_{a1}) \\ i'_{sb} &= \hat{I}_s \sin(\omega_f t + \delta_{b1}) \\ i'_{sc} &= \hat{I}_s \sin(\omega_f t + \delta_{c1}) \end{aligned} \tag{13}$$

where ω_f is the fundamental pulsation of the main voltages given by a Phase Locked Loop (PLL); δ_{a1}, δ_{b1}, and δ_{c1} are the phase shifts of the fundamental main voltages; v_{a1}, v_{b1}, and v_{c1} are equal to 0, $\frac{-2\pi}{3}$, and $\frac{-2\pi}{3}$, respectively if the main voltages are balanced. Theses angles are extracted by a Fourier analysis-based detector. In order to compensate the eventual difference ΔV_{dc} between the voltage V_{C1} and V_{C2} across the two capacitors C_1 and C_2 of the DC-bus, the SAPF is forced to absorb a small DC-term current I_{dc} from the AC source. Thus, if the average capacitor voltage V_{C1} is greater than V_{C2}, a negative DC-term current is added to the line current to compensate capacitor C_2. Conversely, if the average capacitor voltage V_{C2} is greater than V_{C1}, a positive DC-term current is added to the line current to compensate capacitor C_1. Hence, the instantaneous reference source currents are:

$$\begin{aligned} i_{sa}^{*} &= i'_{sa} + I_{dc} \\ i_{sb}^{*} &= i'_{sb} + I_{dc} \\ i_{sc}^{*} &= i'_{sc} + I_{dc.} \end{aligned} \tag{14}$$

The current I_{dc} is computed directly as follows [8]:

$$I_{dc} = K_{dc}(V_{C2} - V_{C1}). \tag{15}$$

To avoid a large DC-term in the source currents, a slight value for the gain K_{dc} is chosen and an eventual limiter can be required. Thus, this method proposes a Proportional-Integral+Proportional (PI+P) actions for V_{dc} and ΔV_{dc} control. Finally, the compensating currents can be obtained from the reference source current and the load currents as follows:

$$\begin{aligned} i_{ca}^{*} &= i_{sa}^{*} - i_{La} \\ i_{cb}^{*} &= i_{sb}^{*} - i_{Lb}. \\ i_{cc}^{*} &= i_{sc}^{*} - i_{Lc} \end{aligned} \tag{16}$$

4. Sliding Mode Control of the Current Loop

The sliding mode control is derived by selecting the suitable switching configuration of the VSI in order to guarantee the state trajectory attraction toward a predefined sliding surface, and to maintain its stability over this surface. The system established in Eq. (7) is a multi-input multi-output non-linear system. In order to formulate the sliding mode creation problem, let:

$$\boldsymbol{x} = [x_1 \quad x_2 \quad x_3 \quad x_4 \quad x_5]^T$$

Subsequently, Eq. (7) can be rearranged as follows [18]:

$$\dot{\boldsymbol{x}} = \boldsymbol{f}(\boldsymbol{x}) + \boldsymbol{G}(\boldsymbol{x})\boldsymbol{u} \tag{17}$$

where $\boldsymbol{f}(\boldsymbol{x})$ is a $(n=5)$-dimensional vector field given as follows:

$$\boldsymbol{f}(\boldsymbol{x}) = \begin{bmatrix} -\frac{r_c}{L_c}x_1 + \frac{1}{2L_c}x_4 - \frac{1}{2L_c}x_5 - \frac{v_a}{L_c} \\ -\frac{r_c}{L_c}x_2 + \frac{1}{2L_c}x_4 - \frac{1}{2L_c}x_5 - \frac{v_a}{L_c} \\ -\frac{r_c}{L_c}x_3 + \frac{1}{2L_c}x_4 - \frac{1}{2L_c}x_5 - \frac{v_a}{L_c} \\ \frac{1}{2C}x_1 + \frac{1}{2C}x_2 + \frac{1}{2C}x_3 \\ -\frac{1}{2C}x_1 - \frac{1}{2C}x_2 - \frac{1}{2C}x_3 \end{bmatrix}.$$

$\boldsymbol{G}(\boldsymbol{x})$ is an $(n \times m = 5 \times 3)$-dimensional input matrix with m n-dimensional vector field given as follows:

$$\boldsymbol{G}(\boldsymbol{x}) = \begin{bmatrix} \frac{x_4+x_5}{2L_c} & 0 & 0 \\ 0 & \frac{x_4+x_5}{2L_c} & 0 \\ 0 & 0 & \frac{x_4+x_5}{2L_c} \\ \frac{x_1}{2C} & \frac{x_2}{2C} & \frac{x_3}{2C} \\ \frac{x_1}{2C} & \frac{x_2}{2C} & \frac{x_3}{2C} \end{bmatrix}.$$

4.1 Sliding surfaces

For the n-dimensional controlled system regulated by m independent switches, m sliding surface coordinate functions are defined. To fast track the reference current, the three sliding surface coordinate functions in vector form are defined as follows:

$$\boldsymbol{\sigma}(\boldsymbol{x}) = \begin{bmatrix}\sigma_1(\boldsymbol{x})\\ \sigma_2(\boldsymbol{x})\\ \sigma_3(\boldsymbol{x})\end{bmatrix} = \begin{bmatrix}x_1 - x_1^*\\ x_2 - x_2^*\\ x_3 - x_3^*\end{bmatrix}. \tag{18}$$

When the sliding mode is reached, in other words, when the state vector is forced to evolve on the intersection of the sliding surfaces, the sliding surface coordinate function $\boldsymbol{\sigma}(\boldsymbol{x})$ must satisfy the following condition:

$$\big(\dot{\boldsymbol{\sigma}}(\boldsymbol{x}), \boldsymbol{\sigma}(\boldsymbol{x})\big) = (\mathbf{0}, \mathbf{0}).$$

Hence, a sliding mode equivalent control denoted by $\boldsymbol{u}_{eq}(\boldsymbol{x})$ may be defined to ensure that the sliding surface coordinate functions $\boldsymbol{\sigma}(\boldsymbol{x})$ satisfy simultaneously the following invariance condition [18]:

$$\dot{\boldsymbol{\sigma}}(\boldsymbol{x}) = \frac{\partial \boldsymbol{\sigma}(\boldsymbol{x})}{\partial \boldsymbol{x}^T}\big(\boldsymbol{f}(\boldsymbol{x}) + \boldsymbol{G}(\boldsymbol{x})\boldsymbol{u}_{\boldsymbol{eq}}(\boldsymbol{x})\big) = \mathbf{0}. \tag{19}$$

We denote $\frac{\partial \boldsymbol{\sigma}(\boldsymbol{x})}{\partial \boldsymbol{x}^T}\boldsymbol{f}(\boldsymbol{x})$ by $\boldsymbol{L}_f(\boldsymbol{x})$, an m-dimensional vector which represents the directional derivatives of $\boldsymbol{\sigma}(\boldsymbol{x})$ along the direction of the vector field $\boldsymbol{f}(\boldsymbol{x})$ as shown in Eq. (20).

$$\boldsymbol{L}_{\boldsymbol{f}}(\boldsymbol{x}) = \begin{bmatrix}\dfrac{\partial \sigma_1(\boldsymbol{x})}{\partial x_1} & \dfrac{\partial \sigma_1(\boldsymbol{x})}{\partial x_2} & \cdots & \dfrac{\partial \sigma_1(\boldsymbol{x})}{\partial x_5}\\ \dfrac{\partial \sigma_2(\boldsymbol{x})}{\partial x_1} & \dfrac{\partial \sigma_2(\boldsymbol{x})}{\partial x_2} & \cdots & \dfrac{\partial \sigma_2(\boldsymbol{x})}{\partial x_5}\\ \dfrac{\partial \sigma_3(\boldsymbol{x})}{\partial x_1} & \dfrac{\partial \sigma_3(\boldsymbol{x})}{\partial x_2} & \cdots & \dfrac{\partial \sigma_3(\boldsymbol{x})}{\partial x_5}\end{bmatrix}\boldsymbol{f}(\boldsymbol{x}) = \begin{bmatrix}\boldsymbol{L}_{f1}(\boldsymbol{x})\\ \boldsymbol{L}_{f2}(\boldsymbol{x})\\ \boldsymbol{L}_{f3}(\boldsymbol{x})\end{bmatrix} \tag{20}$$

where $\boldsymbol{L}_{fj}(\boldsymbol{x})$ ($j = 1, 2, 3$) is the j^{th} component in the vector $\boldsymbol{L}_f(\boldsymbol{x})$.

Similarly, the ($m \times m$)-dimensional matrix $\frac{\partial \boldsymbol{\sigma}(\boldsymbol{x})}{\partial \boldsymbol{x}^T}\boldsymbol{G}(\boldsymbol{x})$ representing the directional derivatives of $\boldsymbol{\sigma}(\boldsymbol{x})$ along the directions of the m vector fields in the matrix $\boldsymbol{G}(\boldsymbol{x})$ is denoted by $\boldsymbol{L}_{\boldsymbol{G}}(\boldsymbol{x})$ as shown in Eq. (21). $\boldsymbol{L}_{\boldsymbol{Gj}}^{l}(\boldsymbol{x})$, $\boldsymbol{L}_{\boldsymbol{Gj}}^{c}(\boldsymbol{x})$ are the j^{th} line and column in the matrix $\boldsymbol{L}_{\boldsymbol{G}}(\boldsymbol{x})$, respectively.

$$\boldsymbol{L}_{\boldsymbol{G}}(\boldsymbol{x}) = \begin{bmatrix}\dfrac{\partial \sigma_1(\boldsymbol{x})}{\partial x_1} & \dfrac{\partial \sigma_1(\boldsymbol{x})}{\partial x_2} & \cdots & \dfrac{\partial \sigma_1(\boldsymbol{x})}{\partial x_5}\\ \dfrac{\partial \sigma_2(\boldsymbol{x})}{\partial x_1} & \dfrac{\partial \sigma_2(\boldsymbol{x})}{\partial x_2} & \cdots & \dfrac{\partial \sigma_2(\boldsymbol{x})}{\partial x_5}\\ \dfrac{\partial \sigma_3(\boldsymbol{x})}{\partial x_1} & \dfrac{\partial \sigma_3(\boldsymbol{x})}{\partial x_2} & \cdots & \dfrac{\partial \sigma_3(\boldsymbol{x})}{\partial x_5}\end{bmatrix}\boldsymbol{G}(\boldsymbol{x}) = \begin{bmatrix}\boldsymbol{L}_{G1}^{l}(\boldsymbol{x})\\ \boldsymbol{L}_{G2}^{l}(\boldsymbol{x})\\ \boldsymbol{L}_{G3}^{l}(\boldsymbol{x})\end{bmatrix} = \begin{bmatrix}\boldsymbol{L}_{G1}^{c}(\boldsymbol{x})\\ \boldsymbol{L}_{G2}^{c}(\boldsymbol{x})\\ \boldsymbol{L}_{G3}^{c}(\boldsymbol{x})\end{bmatrix}^T. \tag{21}$$

Consequently Eq. (19) is rewritten as follows:

$$\dot{\boldsymbol{\sigma}}(\boldsymbol{x}) = \boldsymbol{L}_{\boldsymbol{f}}(\boldsymbol{x}) + \boldsymbol{L}_{\boldsymbol{G}}(\boldsymbol{x})\boldsymbol{u}_{\boldsymbol{eq}}(\boldsymbol{x}) = \mathbf{0}. \tag{22}$$

This permits the definition of the equivalent control in the following form:

$$\boldsymbol{u}_{\boldsymbol{eq}}(\boldsymbol{x}) = -\big(\boldsymbol{L}_{\boldsymbol{G}}(\boldsymbol{x})\big)^{-1}\boldsymbol{L}_{\boldsymbol{f}}(\boldsymbol{x}). \tag{23}$$

This means that, as a condition for the equivalent control definition, the matrix $\boldsymbol{L}_{\boldsymbol{G}}(\boldsymbol{x})$ must be invertible. It should be noted that the equivalent control must satisfy $-\mathbf{1} \le \boldsymbol{u}_{eq}(\boldsymbol{x}) \le \mathbf{1}$, ($\mathbf{1}$ represents an m-dimensional column vector with 1 in each entry) which is a necessary and sufficient condition for the sliding mode existence.

4.2 Sliding surface accessibility

Let us consider the following Lyapunov function:

$$V(\boldsymbol{\sigma}(\boldsymbol{x})) = \frac{1}{2}\boldsymbol{\sigma}^T(\boldsymbol{x})\boldsymbol{\sigma}(\boldsymbol{x}). \tag{24}$$

This positive semi-definite function is identically zero over the surface S, i.e., $\boldsymbol{\sigma}(\boldsymbol{x}) = \mathbf{0}$ and positive when $\boldsymbol{\sigma}(\boldsymbol{x}) \neq \mathbf{0}$. The quantity $V(\boldsymbol{\sigma}(\boldsymbol{x}))$ can be interpreted as the distance from the position of the point $\boldsymbol{x}$ in the state space to the desired surface. Therefore, in order to satisfy the condition $\boldsymbol{\sigma}(\boldsymbol{x}) = \mathbf{0}$, the discrete control $\boldsymbol{u} \in \{-1, 1\}^m$ must exercise a closing or opening action, which permits the decrease in the distance $V(\boldsymbol{\sigma}(\boldsymbol{x}))$, This means that the variation of this function in relation to time must be strictly negative. Consequently:

$$\frac{d}{dt}\big(V(\boldsymbol{\sigma}(\boldsymbol{x}))\big) = \boldsymbol{\sigma}^T(\boldsymbol{x})\dot{\boldsymbol{\sigma}}(\boldsymbol{x}) < 0. \tag{25}$$

This is the condition for the trajectory attraction toward the sliding surface. In Eqs. (22) and (25), if $\boldsymbol{\sigma}(\boldsymbol{x}) \neq \mathbf{0}$, and by replacing $\boldsymbol{u}_{eq}(\boldsymbol{x})$ by $\boldsymbol{u}$, then the time derivative of the Lyapunov function can be expressed as follows:

$$\dot{V}(\boldsymbol{\sigma}(\boldsymbol{x})) = \boldsymbol{\sigma}^T(\boldsymbol{x})\big(\boldsymbol{L}_{\boldsymbol{f}}(\boldsymbol{x}) + \boldsymbol{L}_{\boldsymbol{G}}(\boldsymbol{x})\boldsymbol{u}\big) < 0. \tag{26}$$

Likewise, if $\boldsymbol{\sigma}(\boldsymbol{x}) \neq \mathbf{0}$, then:

$$\dot{V}(\boldsymbol{\sigma}(\boldsymbol{x})) = \boldsymbol{\sigma}^T(\boldsymbol{x})\big(\boldsymbol{L_f}(\boldsymbol{x}) + \boldsymbol{L_G}(\boldsymbol{x})\boldsymbol{u_{eq}}(\boldsymbol{x})\big) = 0. \quad (27)$$

If we consider that the switching frequency is infinite or sufficiently high, we can suppose with good approximation that the state vector x takes the same value in both cases of Eqs. (26) and (27). Thus, replacing $\boldsymbol{\sigma^T}(\boldsymbol{x})\boldsymbol{L_f}(\boldsymbol{x})$ in Eq. (26) by its value from Eq. (27), the restriction in Eq. (25) can be reformulated as follows:

$$\dot{V}(\boldsymbol{\sigma}(\boldsymbol{x})) = \boldsymbol{\sigma}^T(\boldsymbol{x})\boldsymbol{L_G}(\boldsymbol{x})\big(\boldsymbol{u} - \boldsymbol{u_{eq}}(\boldsymbol{x})\big) < 0. \quad (28)$$

Hence, from (21) the following inequality can be deduced:

$$\sum_{j=1,2,3} \boldsymbol{\sigma}^T(\boldsymbol{x})\boldsymbol{L_{Gj}^c}(\boldsymbol{x})u_j < \sum_{j=1,2,3} \boldsymbol{\sigma}^T(\boldsymbol{x})\boldsymbol{L_{Gj}^c}(\boldsymbol{x})u_{eqj}(\boldsymbol{x}) \quad (29)$$

Knowing that $-1 \le \boldsymbol{u_{eqj}}(\boldsymbol{x}) \le 1$, then (29) can be achieved by applying the following control action:

$$u_j = -sign\left(\boldsymbol{\sigma}^T(\boldsymbol{x})\boldsymbol{L_{Gj}^c}(\boldsymbol{x})\right) \quad (30)$$

where $sign$ denotes the sign function.

4.3 Switching frequency

The above expressions are rigorously valid only if we suppose that the system is operating with infinite switching frequency. This is an important constraint in the practical implementation of the sliding mode control. In such application, the switching frequency must be fixed and stabilized at a predefined design value. In order to limit this frequency, a commutation law with fixed hysteresis bandwidth is generally used. Let us suppose that for each restriction, $\boldsymbol{\sigma}_j(\boldsymbol{x}) = \mathbf{0}$ is assigned a hysteresis band $\Delta\boldsymbol{\sigma}_j(\boldsymbol{x})^*$. Therefore, $\boldsymbol{\sigma}_j(\boldsymbol{x})$ oscillates between $\pm\Delta\boldsymbol{\sigma}_j(\boldsymbol{x})^*$, and it is not strictly zero. Consequently, the control defined in Eq. (30) should be redefined as follows:

$$u_j = -sign\left(\Delta\sigma_j(\boldsymbol{x})^* - \boldsymbol{\sigma}^T(\boldsymbol{x})\boldsymbol{L_{Gj}^c}(\boldsymbol{x})\right). \quad (31)$$

Thus, the time derivative of the j^{th} sliding surface coordinate function is:

$$\begin{aligned}\dot{\sigma}_j(\boldsymbol{x}) = \boldsymbol{L_{fj}}(\boldsymbol{x}) + \boldsymbol{L_{Gj}^l}(\boldsymbol{x})sign\Delta\boldsymbol{\sigma}(\boldsymbol{x})^* \\ -\boldsymbol{L_{Gj}^l}(\boldsymbol{x})sign\big(\boldsymbol{\sigma}(\boldsymbol{x})^T\boldsymbol{L_G}(\boldsymbol{x})\big)^T\end{aligned} \quad (32)$$

where $\Delta\boldsymbol{\sigma}(\boldsymbol{x})^* = [\Delta\sigma_1(\boldsymbol{x})^* \quad \Delta\sigma_1(\boldsymbol{x})^* \quad \Delta\sigma_1(\boldsymbol{x})^*]$ which represents the m hysteresis bandwidths assigned for the m surfaces. If we consider that $\Delta\boldsymbol{\sigma}_j(\boldsymbol{x})^*$ are sufficiently slight, the switching frequency is therefore sufficiently high. Thus, we can accept with sufficient approximation that Eq. (32) will be similar to the j^{th} component in Eq. (22) and can be written as:

$$\dot{\sigma}_j(\boldsymbol{x}) = \boldsymbol{L_{fj}}(\boldsymbol{x}) + \boldsymbol{L_{Gj}^l}(\boldsymbol{x})\boldsymbol{u_{eq}}(\boldsymbol{x}) = 0. \quad (33)$$

This means that $\boldsymbol{L_{fj}}(\boldsymbol{x}) = -\boldsymbol{L_{Gj}^l}(\boldsymbol{x})\boldsymbol{u_{eq}}(\boldsymbol{x})$, which replaces the term $\boldsymbol{L_{fj}}(\boldsymbol{x})$ in (32). Thus, the following equations can be deduced:

$$\begin{aligned}\dot{\sigma}_j(\boldsymbol{x}) = \boldsymbol{L_{Gj}^l}(\boldsymbol{x})sign\Delta\boldsymbol{\sigma}(\boldsymbol{x})^* - \boldsymbol{L_{Gj}^l}(\boldsymbol{x})\boldsymbol{u_{eq}}(\boldsymbol{x}) \\ -\boldsymbol{L_{Gj}^l}(\boldsymbol{x})sign\big(\boldsymbol{\sigma}(\boldsymbol{x})^T\boldsymbol{L_G}(\boldsymbol{x})\big)^T\end{aligned}. \quad (34)$$

The new control in Eq. (31) naturally takes two limit values $\{-1, 1\}$, which are needed to reduce the difference $\left|\Delta\sigma_j(\boldsymbol{x})^* - \boldsymbol{\sigma}^T(\boldsymbol{x})\boldsymbol{L_{Gj}^c}(\boldsymbol{x})\right|$ when $\Delta\sigma_j(\boldsymbol{x})^* - \boldsymbol{\sigma}^T(\boldsymbol{x})\boldsymbol{L_{Gj}^c}(\boldsymbol{x})$ is either positive or negative. Consequently, to respect the stability constraint in Eq. (26), Eq. (34) should achieve a positive value in the switched-on interval t_{on} and a negative value in the switched-off t_{off} interval. Therefore, these two intervals can be deduced as follows:

$$t_{on} = \frac{2\Delta\sigma_j(\boldsymbol{x})^*}{\dot{\sigma}_j^+(\boldsymbol{x})} = \frac{2\Delta\sigma_j(\boldsymbol{x})^*}{\boldsymbol{L_{Gj}^l}(\boldsymbol{x})(\mathbf{1} - \boldsymbol{u_{eq}}(\boldsymbol{x}))} \quad (35)$$

$$t_{off} = \frac{2\Delta\sigma_j(\boldsymbol{x})^*}{\dot{\sigma}_j^-(\boldsymbol{x})} = \frac{2\Delta\sigma_j(\boldsymbol{x})^*}{\boldsymbol{L_{Gj}^l}(\boldsymbol{x})\left(\mathbf{1} + \boldsymbol{u_{eq}}(\boldsymbol{x})\right)} \quad (36)$$

where $\dot{\sigma}_j^+(\boldsymbol{x})$ and $\dot{\sigma}_j^-(\boldsymbol{x})$ indicate the positive or negative time derivative of $\dot{\sigma}_j(\boldsymbol{x})$ is positive or negative, respectively.

Knowing that the switching frequency is defined as:

$$f_s = \frac{1}{t_{on} + t_{off}} \quad (37)$$

then, the expression of the switching frequency can be deduced from Eqs. (35) and (36) after simplification as follows:

$$f_s = \frac{\left(\boldsymbol{L_{Gj}^l}(\boldsymbol{x})\mathbf{1}\right) - \left(\boldsymbol{L_{Gj}^l}(\boldsymbol{x})\boldsymbol{u_{eq}}(\boldsymbol{x})\right)^2}{4\Delta\sigma_j(\boldsymbol{x})^*\boldsymbol{L_{Gj}^l}(\boldsymbol{x})\mathbf{1}}. \quad (38)$$

Eq. (38) shows clearly that the switching frequency f_s depends essentially on the equivalent control vector $\boldsymbol{u_{eq}}(\boldsymbol{x})$ and the predefined hysteresis bandwidth $\Delta\boldsymbol{\sigma}_j(\boldsymbol{x})^*$. If this last one is fixed at a slight value, then the switching frequency will be increased. This situation can be recommended for harmonic current control. However, in practical applications, this frequency must take a moderate value to limit switching losses and constraints on power switches, especially when the compensated powers are relatively important. Otherwise, the equivalent control is

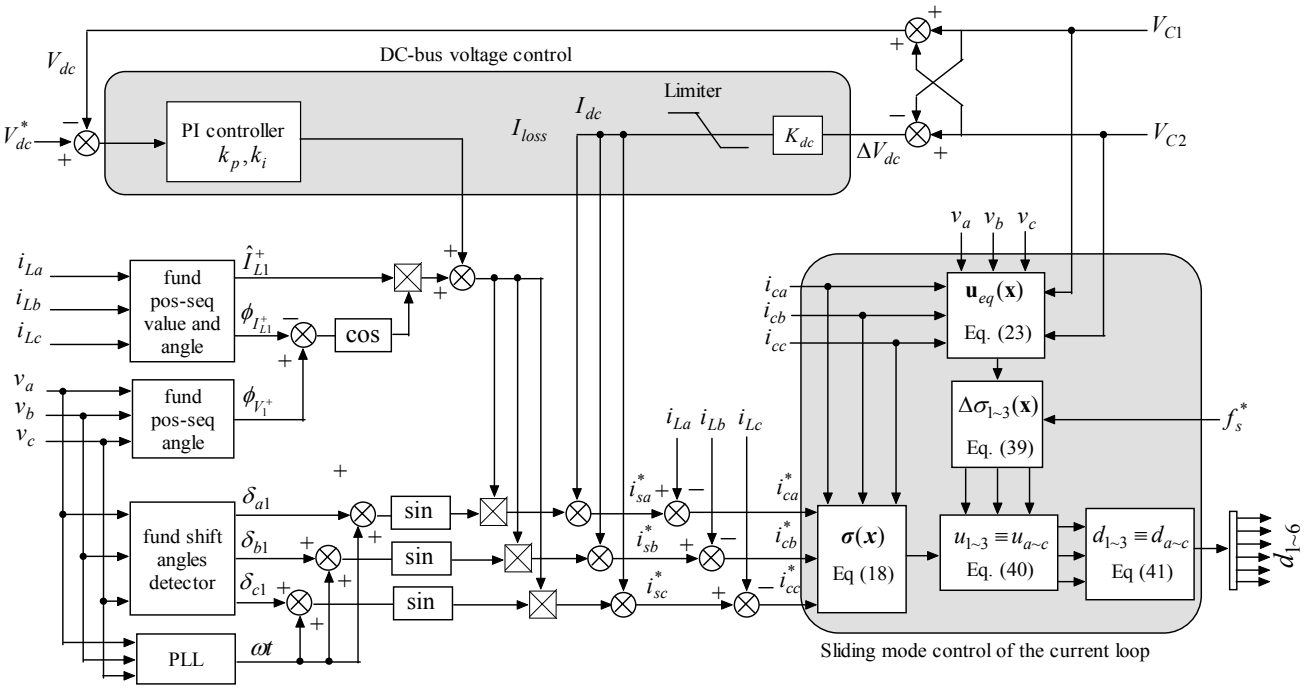

Fig. 2. Complete block diagram of the proposed control

responsible for switching frequency variations, which can cause audible noise and electromagnetic-related problems. In order to solve this problem, the hysteresis bandwidth $\Delta\boldsymbol{\sigma}_j(\boldsymbol{x})$ in the present paper is modulated as a function of the equivalent control $\boldsymbol{u_{eq}}(\boldsymbol{x})$. Thus, this band will change according to the instantaneous value f_s^* of the equivalent control in order to maintain a nearly constant switching frequency at a predefined value. This can be seen in the following equation:

$$\Delta\sigma_j(\boldsymbol{x}) = \frac{\left(\boldsymbol{L}_{\boldsymbol{Gj}}^{\boldsymbol{l}}(\boldsymbol{x})\mathbf{1}\right) - \left(\boldsymbol{L}_{\boldsymbol{Gj}}^{\boldsymbol{l}}(\boldsymbol{x})\boldsymbol{u}_{\boldsymbol{eq}}(\boldsymbol{x})\right)^2}{4f_s^*\boldsymbol{L}_{\boldsymbol{Gj}}^{\boldsymbol{l}}(\boldsymbol{x})\mathbf{1}}. \quad (39)$$

Finally, the discrete controls u_j and d_j are derived as:

$$u_j = -sign\left(\Delta\sigma_j(\boldsymbol{x}) - \boldsymbol{\sigma}^T(\boldsymbol{x})\boldsymbol{L}_{\boldsymbol{Gj}}^{\boldsymbol{c}}(\boldsymbol{x})\right) \quad (40)$$

$$d_j = \frac{1}{2}(1 + u_j). \quad (41)$$

The complete block diagram of the proposed control is shown in Fig. 2.

The performances of the developed sliding mode control are verified through simulation using MATLAB software. The polluting load consists of three-phase thyristor rectifier, single-phase thyristor rectifier, and single-phase diode rectifier. For all the simulations, a load variation is operated at $t = 0.2s$. The main parameters of the system are listed in Table 1.

In Fig. 3, the three-phase and neutral currents are represented with and without active filtering. As illustrated

Table 1. Main parameters of the simulated system

Phase to neutral source voltage	230 *Vrms*, 50 *Hz*
Source inductance	$L_s = 100\ \mu H$
DC-bus capacitors	$C_1 = C_2 = 5\ mF$
DC-bus voltage reference	$V_{dc}^* = 100\ V$
Inductor filter	$L_c = 2\ mH$
Switching frequency reference	$f_s^* = 12.5\ kHz$

in the same figure, harmonic spectra for each phase for the current drawn by the load is unbalanced and contains positive-sequence harmonics $6h+1(7^{th}, 13^{th} \cdots)$, negative-sequence harmonics $6h+5(5^{th}, 11^{th} \cdots)$, and zerosequence harmonics $6h+3(3^{th}, 9^{th} \cdots)$, where h indicates the harmonic order. It should be noted that the zero-sequence harmonics is the result of the 4^{th} wire (neutral). This sequence does not appear in the three-wire systems. With the introduction of the active filtering action, the three-phase current are sinusoidal and balanced, and consequently the current in neutral wire is practically zero. From the current spectra in Fig. 3(d), all the undesired harmonics are almost canceled except for the fundamental positive sequence. The individual harmonics distortions of the other sequence are all less than 1.2% before and after load change. Table 2 summarizes the detailed *THDs* and *rms* values of the currents.

The above results are obtained under the predefined switching frequency of 12.5 *KHz* as predefined switching frequency. Figs. 4 and 5 present a comparison between fixed-frequency and free-frequency sliding mode control performances for two predefined values of the switching

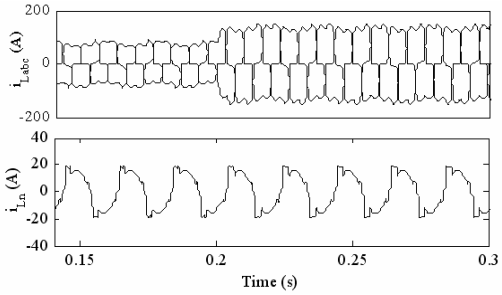

(a) Three-phase and neutral currents without active filtering

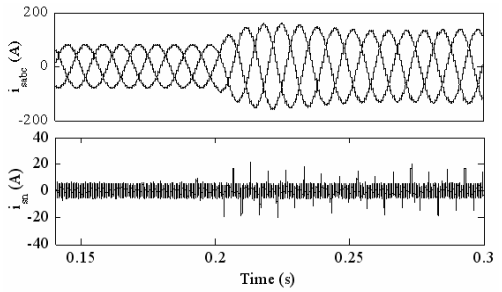

(b) Three-phase and neutral currents with active filtering

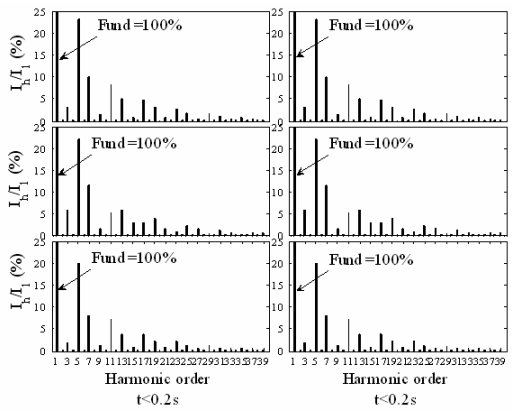

(c) Current spectra for each phase without active filtering before and after load change

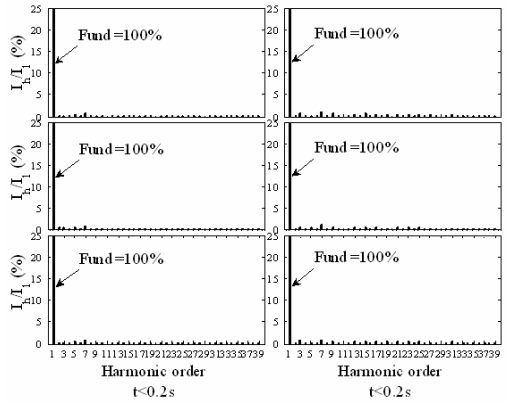

(d) Current spectra for each phase without active filtering before and after load change

Fig. 3. Three-phase currents, neutral currents and current spectra

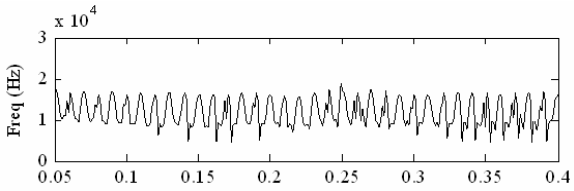

(a) Instantaneous switching frequency with ± 3*A* fixed hysteresis band

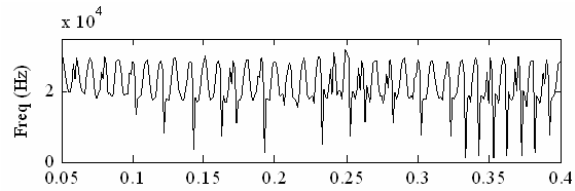

(b) Instantaneous switching frequency with ± 2.5*A* fixed hysteresis band

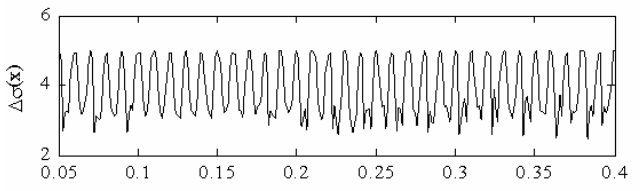

(c) Instantaneous hysteresis bandwidth for 12.5 *KHz* predefined switching frequency

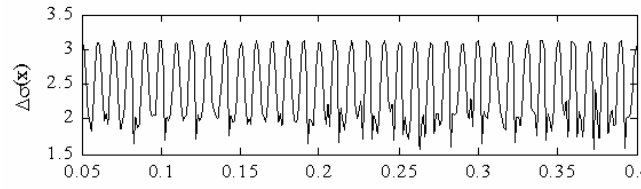

(d) Instantaneous hysteresis bandwidth for 20 *KHz* predefined switching frequency

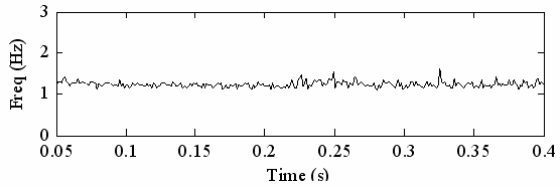

(e) Instantaneous switching frequency for 12.5 *KHz* predefined frequency

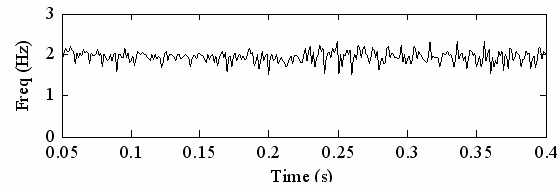

(f) Instantaneous switching frequency for 20 *KHz* predefined frequency

Fig. 4. Switching frequency with free- and fixed-frequency sliding mode control

Table 2. Detailed *THDs* and *rms* values of three-phase and neutral currents before and after active filtering

3-phase, neutral	$t < 0.2s$		$t > 0.2s$	
	Before	After	Before	After
THD (%)				
a-phase	28.29	01.70	26.15	02.53
b-phase	27.67	01.48	24.83	02.00
c-phase	23.76	01.76	23.59	02.09
Neutral	31.31	---	31.31	---
RMS				
a-phase	54.03	54.42	98.42	98.00
b-phase	58.74	54.53	105.57	97.51
c-phase	65.21	54.50	108.57	97.58
Neutral	13.10	---	13.10	---

frequency. The switching frequencies shown in Figs. 4(a) and 4(b) result from a sliding mode control under free-frequency using hysteresis comparators with fixed-bandwidth. The bandwidths are chosen to obtain switching frequency turnaround values of 12.5 *KHz* and 20 *KHz*,. Thus, the hysteresis bandwidths for Fig. 4(a) and Fig. 4(b) are fixed at ± 3*A* and ± 2.5*A*, respectively. The frequencies produce large oscillations (approximately 60% of the average value). For the proposed fixed-frequency, the instantaneous hysteresis bandwidths computed with respect to the previous frequencies and the instantaneous equivalent control are illustrated in Fig. 4(c) and Fig. 4(d), respectively. These bandwidths are not constant; however the instantaneous switching frequencies resulting from these bandwidths are almost constant as shown in Figs. 4(e) and 4(f). Under the same conditions, the source current in the *a*-phase using free-frequency and fixed-frequency control is illustrated in Fig. 5.

The total harmonic distortions are recapitulated in Table 3 which shows that the free-frequency control presents a slight superiority in terms of current tracking. However, no significant difference emerged. The THDs obtained with the two methods are strongly within the standard limits.

Table 3. *a*-phase current THDs with free-frequency and fixed-frequency sliding mode control

	THD (%)	
	$t < 0.2s$	$t > 0.2s$
Fixed-bandwidth ± 3*A*	1.27	2.27
Fixed-frequency 12.5 *KHz*	1.70	2.53
Fixed-bandwidth ± 2.5*A*	1.23	2.26
Fixed-frequency 20 *KHz*	1.43	2.33

6. Conclusion

In the present paper, a sliding mode control under fixed switching frequency of three-phase three-leg voltage source inverter based four-wire shunt active filter using hysteresis comparators to generate the switching signals is achieved. The system is designed to compensate distorted and unbalanced currents under non-ideal main voltages. A

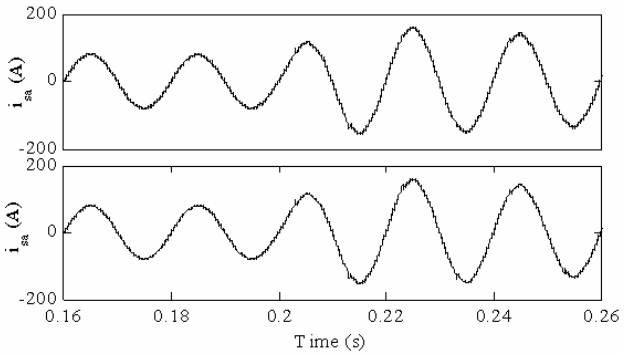

(a) with ± 3*A* fixed-hysteresis band (Top) and with 12.5 *KHz* fixed-frequencym control (bottom).

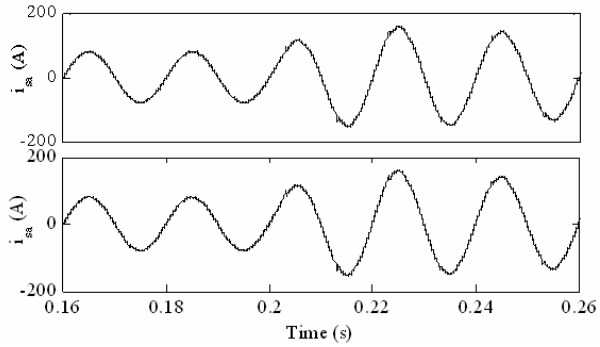

(b) with ± 2.5*A*fixed-hysteresis band (Top) and with 20 *KHz* fixed-frequency control (bottom).

Fig. 5. *a*-phase wave with free- and fixed-frequency sliding mode control

detailed theoretical analysis of sliding mode and the problem of the switching frequency limitation is illustrated in a simple manner. The adopted solution which uses a variable hysteresis band for the switching signals generation has been verified through computer simulation. Very satisfactory results have been obtained which verified that the proposed fixed frequency control can conserve the excellent quality of the free frequency control in terms of current THD improvement by maintaining the switching frequency to a nearly constant value. Therefore, the present control system can be applied successfully to medium or high power electronics converters, such as multilevel structure-based compensators in power system, where a fixed switching frequency is often recommended because of the high power exchange.

References

[1] M. Aredes, J. Häfner, and K. Heulmann, "Three-phase four-wire shunt active filter control strategies", *IEEE Trans. Power. Electron*, vol. 12, no. 02, pp. 311–318, March 1997.

[2] B. Singh, K. Al-Haddad, and A. Chandra, "Harmonic elimination, reactive power compensation and load balancing in three-phase, four-wire electric distribution systems supplying non-linear loads", *Electric Power Syst. Res*, vol. 44, pp. 93–100, 1998.

[3] Singh, K. Al-Haddad, and A. Chandra, "A review of active filters for power quality improvement,", *IEEE Trans. Ind. Electron*, vol. 46, no. 5, pp. 960–971, 1999.

[4] Madtharad and S. Premrudeepreechacharn, "Active power filter for three-phase four-wire electric systems using neural networks", *Electric Power Syst. Res*, vol. 60, pp. 177–192, 2002.

[5] A. Cavini, F. Ronchi, and A. Tilli, "Four-wires shunt active filters: optimized design methodology", *in Industrial Electronics Society. The 29th Annual Conference of the IEEE*, 2003, pp. 2288–2293.

[6] B. Lin, H. Chiang, and K. Yang, "Shunt active filter with three-phase four-wire npc inverter", *in IEEE. The 47th IEEE International Midwest Symposium on Circuits and Systems*, 2004, pp. 281–284.

[7] M. Benhabib and S. Saadate, "New control approach for four-wire active power filter based on the use of synchronous reference frame", *Electric Power Syst. Res,* vol. 73, pp. 353–362, 2005.

[8] B. Lin and T. Y. Yang, "Analysis and implementation of three-phase power quality compensator under the balanced and unbalanced load conditions", *Electric Power Syst Res*, vol. 76, pp. 271–282, 2006.

[9] M. Ucar and E. Ozdemir, "Control of a 3-phase 4-leg active power filter under non-ideal mains voltage condition," *Electric Power Syst Res*., 2007.

[10] D. Boroyevich, F. C. Lee, R. Zhang, and V. H. Prasad, "Three dimensional space vector madulatin for four-leg voltage-source conveners", *IEEE trans. power. electronics*, vol. 17, no. 3, 2002.

[11] H. Akagi, Y. Kanazawa, and A. Nabae, "Generalized theory of the instantaneous reactive power in three-phase circuits", *in IPEC'83- Int. Power Elec. Conf*, Tokyo, Japan, 1983, pp. 1375–1386.

[12] V. Siares and P. Verdelho, "Analysis of active power filters in frequency domain using the fast Fourier transform", *EPE*, 1997.

[13] H. Bühler, *Réglage par mode de glissement. Lausane, Suisse*, Presse Polytechnique Romandes, 1986.

[14] N. Sabanovic, T. Ninomiya, A. Sabanovic, and B. Perunicic, "Control of three-phase switching converters: A sliding mode approach", *PESC* 1993.

[15] G. Spiazzi, P. Mattavelli, L. Rossetto, and L. Alesani, "Application of sliding mode control to switch-mode power supplies", *Journal of Circuits, Systems and Computers (JCSC)*, vol. 5, no. 3, pp. 337–354, 1995.

[16] V. Utkin, J. Guldner, and J. Shi, *Sliding Mode Control in Electromechanical Systems. London*: Taylor and Francis, 1999.

[17] M. Ahmed, "Sliding mode control for switched mode power supplies" *Ph.D thesis*, Lappeenranta University of Technology, Finland, 2004.

[18] H. Sira-Ramirez and R. Silva-Ortigoza, *Control Design Techniques in Power Electronics Devices*. London: Springer-Verlag, 2006.

[19] S.Guffon, A. Toledo, S.Bacha, and G.Bornard, "Indirect sliding mode control of a three-phase active power filter", *IEEE*, 1998, pp. 1408–1414.

[20] N. Mendalek, K. Al-Haddad, F. Fnaiech, and L. A. Dessaint, "Sliding mode control of 3-phase 3-wire shunt active filter in the dq-frame", *CCECE. IEEE*, 2001, pp. 765–770.

[21] B. Lin, Z. Hung, S. Tsay, and M. Liao, "Shunt active filter with sliding mode control", *IEEE*, 2001, pp. 884–889.

[22] B. Bose, "An adaptive hysteresis-band current control technique of a voltage fed pwm inverter for machine drive system", *IEEE Trans. Ind. Electron*, vol. 37, pp. 402–408, 1990.

[23] L. A. Moran, J. W. Dixon, and R. R. Wallace, "A three-phase active power filer operating with fixed switching frequency for reactive power and current harmonic compensation", *IEEE Trans. Ind. Electron*, vol. 42, no. 4, pp. 402–408, 1995.

[24] V. Nguyen and C. Lee, "Tracking control of buck converter using sliding mode with adaptive hysteresis", *in 26th Power Electronics Specialists Conference*, Atlanta, USA, 1995, pp. 1086–1093.

[25] J. Zeng, C. Yu, Q. Qi, Z. Yan, Y. Ni, B. Zhang, S. Chen, and F. F. Wu, "A novel hysteresis current control for active power filter with constant frequency", *Electric Power Syst. Res*, vol. 68, pp. 75–82, 2004.

[26] M. Kale and E. Ozdemir, "An adaptive hysteresis band current controller for shunt active power filters", *Electric Power Syst. Res*, vol. 73, pp. 113–119, 2005.

[27] B. Mazari and F. Mekri, "Fuzzy hysteresis control and parameter optimization of a shunt active filter", *Journal of Information Science and Engineering*, vol. 21, pp. 1139–1156, 2005.

[28] M. Navarro-Lopez, D. Cortés, and C. Castro, "Design of practical sliding-mode controllers with constant switching frequency for power converters", *Electric Power Syst Res*, vol. 79, pp. 796–802, 2009.

[29] S. Tan, Y. Lai, and C. Tse, "Implementation of pulse-width-modulation based sliding mode controller for boost converters", *IEEE Power Electron*, vol. 3, no. 4, pp. 130–135, 2006.

[30] S. Buso, L. Malesani, and P. Mattavelli, "Comparison of current control techniques for active filter applications", *IEEE Trans. Power. Electron* vol. 45, no. 5, pp. 722–729, 1998.

[31] I. Etxeberria-Otadui, "Sur les systèmes de l'électronique de puissance dédiés à la distribution électrique-application à la qualité de l'énergie", *Ph.D. dissertation*, INPG, Grenoble, France, September

2003.

[32] M. Aredes and E. Watanabe, "New control algorithms for series and shunt three-phase four-wire active power filters", *IEEE Transactions on Power Delivery*, vol. 10, no. 3, pp. 1649–1656, July 1995.

Farid Hamoudi received his engineering degree from the University of Bejaia, Algeria and the Master's degree from the University of Batna, Algeria in 2005 and 2008, respectively. Currently, he is a PhD student at the University of Batna. His research interests include modeling and control of power electronic-based systems for power quality improvement in electric distribution systems. Since December 2009, he has served as assistant professor at the Institute of Electrical and Electronic Engineering at the University of Boumerdès, Algeria.